PROCEEDINGS OF SCIENCE

Color screening in lattice QCD and at weak coupling

Johannes Heinrich Weber* **[TUMQCD collaboration]**

Technische Universität München
E-mail: johannes.weber@tum.de

We study spatial correlation functions of static quark-antiquark pairs in QCD with 2+1 flavors in order to better understand color screening at high temperatures. We performed lattice simulations in a wide temperature window $115\,\mathrm{MeV} \lesssim T \lesssim 5.8\,\mathrm{GeV}$ using the using the highly improved staggered quark (HISQ) action, the tree-level improved Symanzik gauge action and several lattice spacings to control discretization effects. By comparing our lattice results to analytic calculations at weak coupling as well as to the zero temperature result on the static energy we demonstrate that color screening sets in at distances $rT \simeq 0.25$. We also conclude that in the distance regime $0.25 < rT < 0.6$ the weak-coupling approach provides an adequate description of color screening.

Critical Point and Onset of Deconfinement - CPOD2017
7-11 August, 2017
The Wang Center, Stony Brook University, Stony Brook, NY

*Speaker.

PoS(CPOD2017)083

1. Introduction

It is known from quantum field theoretical studies as well as from heavy-ion collision experiments at RHIC, GSI or LHC and astronomical observations of neutron stars that strongly interacting matter exhibits very different properties depending on the temperature and the baryon density. For sufficiently small values of the baryochemical potential a high temperature phase called quark-gluon-plasma has been established. Distinctive properties of quark-gluon-plasma are color screening, deconfinement and restoration of chiral symmetry, cf. recent reviews [1, 2].

In the limit of vanishing sea quark masses or in the limit of zero flavors of sea quarks, the transition between quark-gluon-plasma and the vacuum is sharp. For pure gauge theory and the gauge group SU(N_c), the Polyakov loop is the order parameter of a deconfinement transition, which is related to the spontaneous breaking of the Z(N_c) center symmetry of the Yang-Mills vacuum. Since the center symmetry is broken by the presence of sea quarks with sufficiently small quark masses already in the hadronic phase, the Polyakov loop does not play the role of an order parameter in full QCD. For massless sea quarks, the chiral susceptibility is the order parameter of the chiral phase transition. For sufficiently large sea quark masses, the chiral symmetry is already broken explicitly by the quark masses and the chiral susceptibility does not play the role of an order parameter in full QCD. In an intermediate range of sea quark masses that includes the physical point, neither is an order parameter and the QCD transition is a crossover. Nevertheless, would-be order parameters still provide insight into the mechanisms of breaking the associated approximate symmetries.

Polyakov loops and correlators of Polyakov loops are observables that are sensitive to color screening. After proper renormalization the Polyakov loop correlator C_P can be regarded as the correlator of a heavy quark-antiquark pair in the limit of infinite heavy quark mass. C_P is related to the free energy of a static $Q\bar{Q}$ pair separated by r, namely $C_P(r,T) = \exp\left[-F_{Q\bar{Q}}(r,T)/T\right]$. In the following we report on preliminary results of a forthcoming extensive analysis of Polyakov loop correlators in lattice QCD with 2+1 flavors of sea quarks [3].

2. Setup

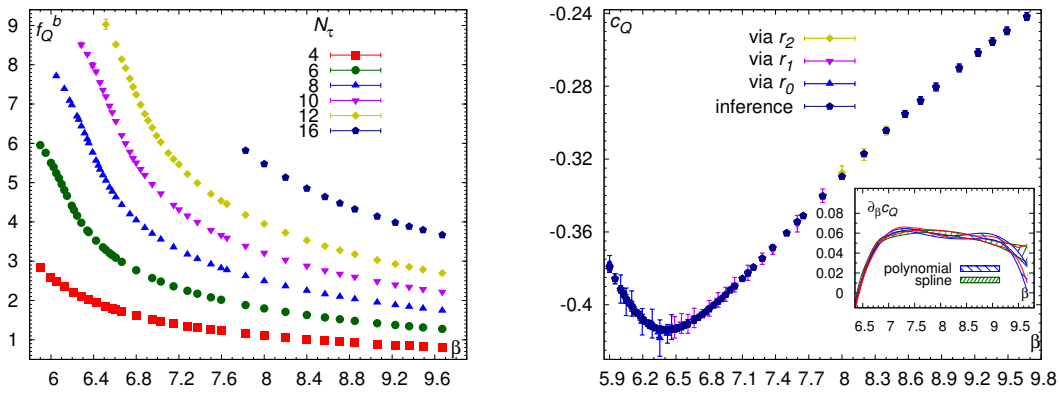

Figure 1: Combined TUMQCD and HotQCD 2+1 flavor gauge ensembles in terms of the bare free energy f_Q^b (left). The renormalization constant c_Q from direct renormalization supersedes the old result [6] (right).

We perform simulations of QCD with 2+1 flavors of sea quarks and calculate the Polyakov loop correlator as well as the color-singlet correlator of a static $Q\bar{Q}$ pair in Coulomb gauge. For our simulations we use the MILC code. We employ the highly improved staggered quark (HISQ) action and tree-level improved Symanzik gauge action. The gauge ensembles have been generated by the HotQCD and TUMQCD collaborations [3, 4, 5, 6]. A detailed account of all ensembles is given in [3]. We use lattices with extensions ${N_\sigma}^3 \times N_\tau$ or ${N_\sigma}^2 \times N_z \times N_\tau$. For the temporal extent we use $N_\tau = 16,\ 12,\ 10,\ 8,\ 6$ and 4, for the spatial extent we choose $N_\sigma/N_\tau = 4$ and 6. We also use a few ensembles with $N_z = 2N_\sigma$. We set the strange quark mass m_s to its physical value and use a degenerate light quark doublet with $m_l = m_s/20$ or $m_l = m_s/5$. These choices correspond in the continuum limit to pion masses of $m_\pi \approx 160$ or 320 MeV respectively. We fix the strange quark mass in terms of the hypothetical $\eta_{s\bar{s}}$ meson, $m_{s\bar{s}} \approx 695$ MeV, or if determination on $T = 0$ lattices with the same parameters is not possible, through the lattice mass renormalization function determined in [5]. We fix the lattice spacing using the r_1 scale and the non-perturbative β function defined in [7]. The scale parameters $r_0,\ r_1$ and r_2 are defined in terms of the $T = 0$ static energy V_S and the corresponding force,

$$r^2 \left.\frac{dV_S}{dr}\right|_{r=r_0} = 1.65, \qquad r^2 \left.\frac{dV_S}{dr}\right|_{r=r_1} = 1, \qquad r^2 \left.\frac{dV_S}{dr}\right|_{r=r_2} = \frac{1}{2}. \tag{2.1}$$

We obtain r_1 from r_0 on coarser lattices and from r_2 on finer lattices. The bare gauge couplings $\beta = 10/g_0^2$ that we use are in the range of $5.9 \leq \beta \leq 9.67$, which corresponds to lattice spacings of $a \approx 0.0085$ to 0.25 fm. We have about 30 different values of β available for each N_τ except $N_\tau = 16$. A chart of the combined TUMQCD and HotQCD ensembles is shown in the left panel of Fig. 1. Therefore, our simulations span the temperature range between $T \approx 115$ and 5814 MeV. The full temperature interval between 134 and 2326 MeV is covered by at least four different N_τ.

All of our $T > 0$ ensembles with $m_l = m_s/5$ have temperatures of at least $T \approx 350$ MeV such that the quark mass dependence is very mild. We observe that Polyakov loops and the correlators in ensembles with different quark masses are numerically compatible within uncertainties, although most $m_l = m_s/5$ ensembles have smaller statistical uncertainties. If both are available we choose the ensemble with better signal-to-noise ratio and combine ensembles with different m_l into a common data set. We use the same r_1 scale independent of the quark mass, since the r_1 for both setups is known to differ by only about 1%[7], which is hardly relevant for our study.

We calculate the bare Wilson line W, the bare Polyakov loop P and the corresponding bare Polyakov loop expectation value L^{b} as

$$W(N_\tau, \boldsymbol{x}) = \prod_{\tau=1}^{aN_\tau} U^0(\tau, \boldsymbol{x}), \qquad P(N_\tau, \boldsymbol{x}) = \frac{1}{3}\mathrm{Tr}_c W(N_\tau, \boldsymbol{x}), \qquad L^{\mathrm{b}}(\beta, N_\tau) = \langle P(N_\tau, \boldsymbol{x})\rangle_\beta\,, \tag{2.2}$$

where we average over the full volume before taking the ensemble average denoted through the angle brackets $\langle\ldots\rangle_\beta$. $L^{\mathrm{b}} \equiv L^{\mathrm{b}}_F$ is the Polyakov loop in the fundamental representation. We renormalize the Polyakov loop through $L(\beta, N_\tau) = \exp[aC_Q(\beta)N_\tau]L^{\mathrm{b}}(\beta, N_\tau)$, where C_Q is a renormalization constant that removes the self-energy divergence due to the gauge links U^0. We obtain C_Q from the $T = 0$ static energy V_S at $r = r_0,\ r_1$ or r_2 for $\beta \leq 8.4$ and extend it to $\beta > 8.4$ using direct renormalization as described in [6]. We require only one iteration of direct renormalization

owing to the enlarged data set. In the right panel of Fig. 1 we show that the uncertainties of C_Q for $7.03 < \beta < 8.85$ are much reduced due to the inference between six different N_τ in the direct renormalization procedure thanks to the new $T = 0$ lattices with $\beta \geq 8.0$ and thanks to the new high temperature lattices with $N_\tau > 8$ and $\beta > 8.4$. We obtain the free energy of an isolated static quark as $F_Q(T,a) = -T \ln L(\beta, N_\tau)$. In free energies we trade β and N_τ for the physical temperature $T = 1/(aN_\tau)$ and the lattice spacing a. The expectation values of the bare correlators are

$$C_P^{\mathrm{b}}(\beta, N_\tau, r) = \left\langle P(N_\tau, \boldsymbol{x}) P^\dagger(N_\tau, \boldsymbol{x}+\boldsymbol{r}) \right\rangle_\beta , \tag{2.3}$$

$$C_S^{\mathrm{b}}(\beta, N_\tau, r) = \frac{1}{3} \left\langle \mathrm{Tr}_c \left\{ W(N_\tau, \boldsymbol{x}) W^\dagger(N_\tau, \boldsymbol{x}+\boldsymbol{r}) \right\} \right\rangle_\beta . \tag{2.4}$$

For Eq. (2.4) we have fixed Coulomb gauge and the trace $\mathrm{Tr}_c\{\ldots\}$ runs over all color indices. We average the correlators over the full volume before taking the ensemble average. We may interpret Eq. (2.4) as a static meson correlation function at Euclidean time $\tau = 1/T$ with a separation r between the quark and antiquark. In the infinite volume limit the static $Q\bar{Q}$ decouple and the correlators approach $|L^{\mathrm{b}}(\beta, N_\tau)|^2$ [1]. The self-energy divergences due to the gauge links U^0 contributing to the Polyakov loop and the correlators cancel exactly in the ratios

$$C_P^{\mathrm{sub}}(\beta, N_\tau, r) = \left\langle \frac{\langle P(N_\tau, \boldsymbol{x}) P^\dagger(N_\tau, \boldsymbol{x}+\boldsymbol{r}) \rangle_{\boldsymbol{x}}}{\langle P(N_\tau, \boldsymbol{x}) \rangle_{\boldsymbol{x}}^2} \right\rangle_\beta , \tag{2.5}$$

$$C_S^{\mathrm{sub}}(\beta, N_\tau, r) = \frac{1}{3} \left\langle \frac{\langle \mathrm{Tr}_c \left\{ W(N_\tau, \boldsymbol{x}) W^\dagger(N_\tau, \boldsymbol{x}+\boldsymbol{r}) \right\} \rangle_{\boldsymbol{x}}}{\langle P(N_\tau, \boldsymbol{x}) \rangle_{\boldsymbol{x}}^2} \right\rangle_\beta , \tag{2.6}$$

which are do not require renormalization. Here we explicitly separate the volume average $\langle \ldots \rangle_{\boldsymbol{x}}$ and the ensemble average $\langle \ldots \rangle_\beta$, taking the ratios along the molecular dynamics history to benefit from partial cancellation of statistical fluctuations between the correlators for large $Q\bar{Q}$ separations and the Polyakov loops. We define subtracted free energies in terms of these ratios,

$$F_{Q\bar{Q}}^{\mathrm{sub}}(r,T,a) = -T \ln C_P^{\mathrm{sub}}(\beta, N_\tau, r), \qquad F_S^{\mathrm{sub}}(r,T,a) = -T \ln C_S^{\mathrm{sub}}(\beta, N_\tau, r). \tag{2.7}$$

By adding $2F_Q(T,a)$ we obtain renormalized free energies $F_{Q\bar{Q}} = F_{Q\bar{Q}}^{\mathrm{sub}} + 2F_Q$ and $F_S = F_S^{\mathrm{sub}} + 2F_Q$. We denote any free energies in the following just by F if no distinction is required and write for F in units of the temperature $f = F/T$. Similarly we write for the renormalization constant times the lattice spacing $c_Q = aC_Q$, cf. Fig. 1.

3. Lattice results

In this section we discuss the main results of our lattice calculation. The free energies F are available only for discrete sets of temperatures that are different for each N_τ. Moreover, for fixed temperature $T = 1/(aN_\tau)$ the available separations r or rT are not the same for data with different N_τ. This is particularly relevant as we use tree-level and non-perturbative improvement [3] for the correlators. Lastly, we observe that the cutoff effects are strongly rT and T dependent. These issues necessitate either a fully global analysis in rT, T and a or subsequent interpolations in rT and T

[1] For QCD this is simply $(L^{\mathrm{b}}(\beta, N_\tau))^2$ since L is real.

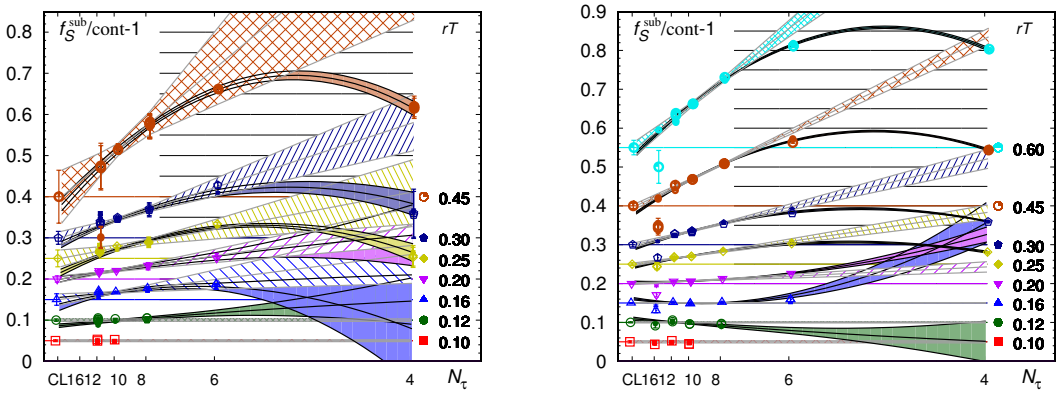

Figure 2: Scaling behavior of $F_S^{\rm sub}$ for $T = 200$ and 800 MeV (from left to right). Larger open symbols indicate results from successive local interpolations, smaller filled symbols from global fits in rT and T. Data have been normalized by the continuum limit and shifted vertically for better visibility. $F_{Q\bar{Q}}$ and F_S follow the same overall trends in the scaling behavior.

followed by extrapolations in a or $1/N_\tau$ respectively. We pursue both approaches, performing first a full Jackknife analysis for each $F(T,a)$ to interpolate in rT and then a temperature interpolation for each $F(rT,a)$ using smoothing splines with the bootstrap method for error propagation. Alternatively we perform global fits for each $F(N_\tau)$ restricted to overlapping low or high temperature intervals using the bootstrap method. As the results are largely commensurate we average over both and estimate systematic uncertainties from their difference. Eventually we extrapolate each $F^{\rm sub}(rT,T)$ to the continuum limit using different assumptions on scaling behavior, namely

$$F^{\rm sub}(rT,T,N_\tau) = F_0^{\rm sub}(rT,T) + \frac{F_2^{\rm sub}(rT,T)}{{N_\tau}^2} + \frac{F_4^{\rm sub}(rT,T)}{{N_\tau}^4} \tag{3.1}$$

with or without the quadratic and quartic terms and for different restrictions of the N_τ range. We generally find that discretization errors are more prominent for larger rT and for lower temperatures as we show in Fig. 2. Data for $N_\tau = 6$ are in the a^2 scaling regime except for $T < 200$ MeV or $rT > 0.3$, while data for $N_\tau = 4$ always require a^4 scaling. In the range of $rT \leq 0.15$ and $T \geq 180$ MeV data for $N_\tau \geq 8$ are within uncertainties consistent with the continuum limit. We piece together the continuum result from appropriate continuum extrapolations for each (rT,T) range and finally renormalize by adding $2F_Q(T)$ to the continuum limit.

We show the continuum limit of F_S and $F_{Q\bar{Q}}$ in Fig. 3. We observe for $T \gtrsim 300$ MeV that the free energies reach their asymptotic value $2F_Q$ within errors. For separations up to $rT \lesssim 0.25$ the difference between the $T = 0$ static energy V_S and the $T > 0$ singlet free energy F_S is small compared to the uncertainty of the renormalization constant $2C_Q$. For sufficiently small separations $F_{Q\bar{Q}} - T\ln(9)$ is numerically consistent with F_S as suggested by the gauge-dependent color decomposition [9]

$$C_P(rT,T) = \exp\left[-F_{Q\bar{Q}}(rT,T)/T\right] = \frac{1}{9}\exp\left[-F_S(rT,T)/T\right] + \frac{8}{9}\exp\left[-F_A(rT,T)/T\right]. \tag{3.2}$$

4. Vacuum-like regime

It is clear that free energies depend only mildly on effects of the thermal medium at sufficiently

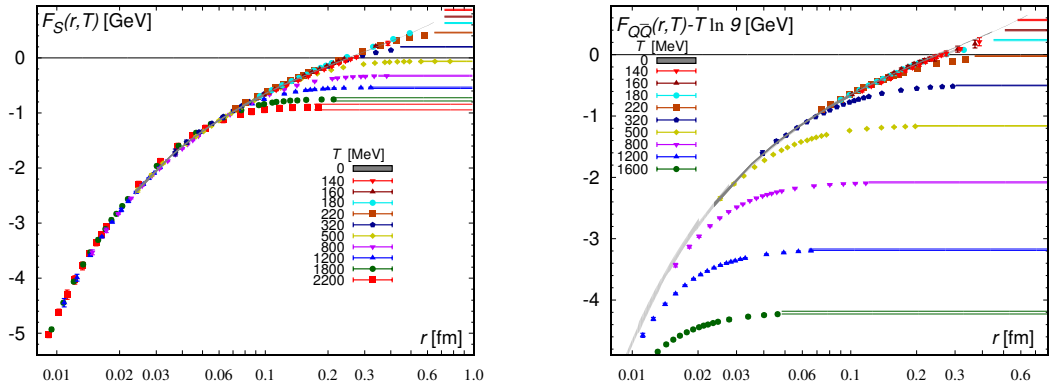

Figure 3: Continuum limit of F_S (left) and $F_{Q\bar{Q}}$ (right). We show V_S at $T=0$ as a dark gray band and F_S for $rt<0.25$ as a light gray band. The colored lines indicate $2F_Q$ (left) or $2F_Q - T\ln 9$ (right) respectively.

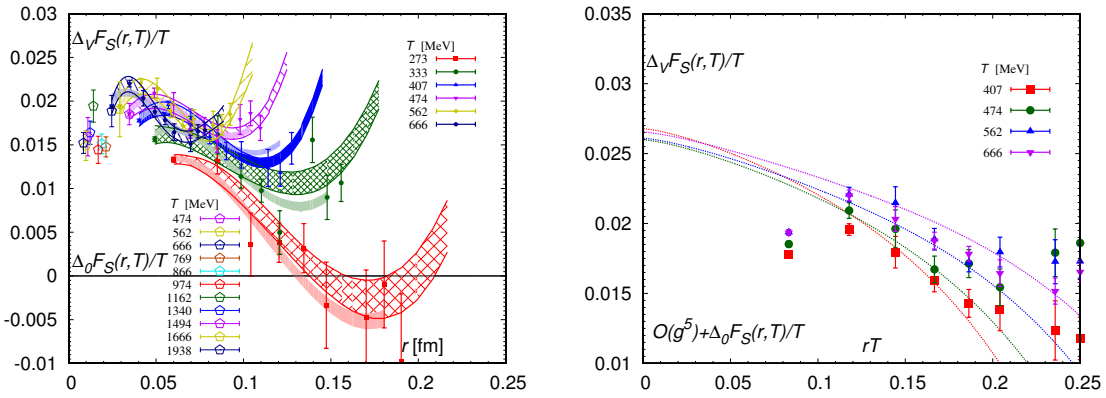

Figure 4: In the vacuum-like regime $\Delta_V F_S$ and $\Delta_0 F_S$ are commensurable (left). Up to a shift of similar size as $\Delta_0 F_S$ the rT dependence is consistent with the pNRQCD prediction at $\mathcal{O}(g^5)$ shown as lines (right).

small separations. Thanks to asymptotic freedom small separations imply weak coupling. Thus, there may be a regime where weak coupling and lattice QCD results are compatible.

The difference $\Delta_V F_S = V_S - F_S$ is particularly suitable for a comparison between both approaches. Namely, the self-energy divergences in $\Delta_V F_S$ cancel exactly, thus alleviating the need for renormalization with C_Q and the associated error. Moreover, as discretization errors for $r/a \lesssim 3$ due to the breaking of rotational symmetry in V_S and F_S are similar, $\Delta_V F_S$ benefits from a strong compensation of errors. $\Delta_V F_S$ has been calculated in pNRQCD up to $\mathcal{O}(\alpha_s^3)$ [8]. The result reads

$$\Delta_V F_S(rT,T) \equiv V_S(r) - F_S(rT,T) = \alpha_s^2 T\left[\Delta f_g(rT) + \Delta f_f(rT) + \Delta f_s(rT,g)\right] + \mathcal{O}(\alpha_s^3). \tag{4.1}$$

Gluonic, fermionic and screening terms Δf_g, Δf_f and Δf_s read as functions of $x = (\pi/3)rT$

$$\Delta f_g(x) = N_c C_F\left\{-\frac{1}{3}x + \frac{2\zeta(3)}{\zeta(2)}x^2 - \frac{22}{25}x^3\right\} + \mathcal{O}(\alpha_s, x^4), \tag{4.2}$$

$$\Delta f_f(x) = N_f C_F\left\{+\frac{3\zeta(3)}{2\zeta(2)}x^2 - \frac{7}{10}x^3\right\} + \mathcal{O}(\alpha_s, x^4)), \tag{4.3}$$

$$\Delta f_s(x) = -\frac{C_F}{\alpha_s}\left(\frac{m_D^{LO}}{T}\right)^3 \frac{1}{4\zeta(2)}x^2 + \mathcal{O}(g^3 x^4). \tag{4.4}$$

$m_D^{LO} = gT\sqrt{(N_c+N_f/2)/3}$ is the leading order Debye mass. The coefficients of x^2 in Δf_g and Δf_f on the one hand and Δf_s on the other hand have opposite sign, indicating a compensation between different thermal effects.

We take note that on dimensional grounds F_S may contain an rT independent term[2] of order $\alpha_s^3 T$. We denote this term as $\Delta_0 F_S(T)$ and determine it at the smallest available distance, $r/a = 1$,

$$\Delta_0 F_S(T) = \lim_{a\to 0}\lim_{r\to 0}\left\{F_S(r,T,a) - \lim_{T\to 0} F_S(r,T,a)\right\} \approx \left\{F_S(\frac{1}{a},T,a) - \lim_{N_\tau\to\infty} F_S(\frac{1}{a},\frac{1}{aN_\tau},a)\right\}. \quad (4.5)$$

We calculate $\Delta_0 F_S(T)$ for fixed lattice spacing a through Eq. (4.5) using only $N_\tau \geq 10$ and find no systematic a dependence. Thus, we consider $\Delta F_S(1/a,T,a)$ as continuum estimate for $\Delta_0 F_S(T)$. Using $N_\tau = 12$ data we show in Fig. 4 the lattice results for $\Delta_V F_S$ and $\Delta_0 F_S$ together in the left panel and with the weak-coupling results in the right panel. Below $rT \lesssim 0.25$ $\Delta_V F_S$ is small and only mildly rT dependent, about 2% of the temperature, while above $rT \gtrsim 0.25$ temperature effects in $\Delta_V F_S$ rapidly become large, giving rise to a steep rT dependence due to color screening.

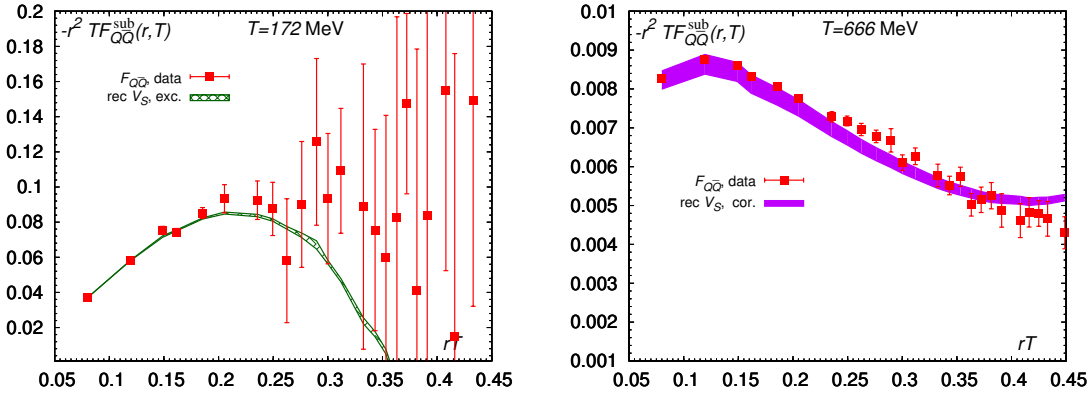

Figure 5: In the vacuum-like regime pNRQCD describes $F_{Q\bar{Q}}$ in terms of V_S, V_A and L_A. $F_{Q\bar{Q}}$ is insensitive to V_A and L_A for $T < 200\,\mathrm{MeV}$ (left), while both and Eq. (4.7) must be included at high temperatures (right).

In weakly-coupled pNRQCD the Polyakov loop correlator satisfies at small separations a gauge-invariant decomposition in terms of singlet and adjoint free energies [10], which is reminiscent of Eq. (3.2). Up to higher orders in rT and rm_D this is a relation with singlet and adjoint potentials, V_S and V_A, and the Polyakov loop in the adjoint representation, L_A. Namely,

$$C_P(rT,T) = \exp\left[-F_{Q\bar{Q}}(rT,T)/T\right] = \frac{1}{N_c^2}\exp\left[-V_S(r)/T\right] + \frac{N_c^2-1}{N_c^2}L_A(T)\exp\left[-V_A(r)/T\right]. \quad (4.6)$$

We obtain the adjoint potential V_A from V_S by including the Casimir-scaling violation [11]

$$(N_c^2-1)V_A + V_S = N_c\frac{N_c^2-1}{8}\frac{\alpha_s^3}{r}\left(\pi^2/4-3\right) + \mathcal{O}(\alpha_s^4). \quad (4.7)$$

Via Casimir scaling we obtain $L_A = [(1-\delta_8)L_F]^{C_F/C_A}$. Casimir-scaling violations are parameterized by δ_8, which is empirically compatible with zero for $T > 300\,\mathrm{MeV}$ [12]. Using $N_\tau = 12$ data we show in Fig. 5 that $F_{Q\bar{Q}}$ is described well by Eq. (4.6) up to $rT \lesssim 1/3$. In particular, we do not

[2]The rT independence is supposed to hold only for the leading order, i.e. α_s^3.

see significant differences between Eq. (4.6) including or excluding the V_A contribution for $T < 200\,\mathrm{MeV}$, indicating that the color-adjoint contribution is suppressed. This is contrasted by a poor reconstruction of $F_{Q\bar{Q}}$ at high temperatures without correction via Eq. (4.7). Hence, cancellation between color-singlet and -adjoint states becomes stronger with increasing temperature, or in other words, the spectral gap shrinks. This lowered gap suggests that real-time processes like dissociation and recombination may be dominant for compact heavy quark-antiquark systems in a thermal bath.

5. Electric screening regime

For $Q\bar{Q}$ separations larger than $rT \gtrsim 0.25$ the correlators invariably become more and more sensitive to the color screening. In this section we establish whether this can be related to the Debye screening in dimensionally-reduced effective field theories. These can be obtained for quantum field theories at sufficiently high temperatures by integrating out the non-static Matsubara modes through a UV cutoff [13]. The three-dimensional effective theory for QCD is called electrostatic QCD (EQCD) [14]. Its low-energy degree of freedom is the electrostatic gauge field, whose mass parameter corresponds to the perturbative Debye mass. Since the running of the gauge coupling in EQCD is far milder than for QCD, we anticipate a regime around $rm_D \sim 1$ with moderately weak interactions even at values of r where confinement would be observable in the vacuum.

Both the free energy [9] and the singlet free energy [15] have been calculated in EQCD at NLO in terms of the Debye mass. For consistent counting we require m_D determined at NLO [14],

$$(m_D^{NLO})^2 = \left(1 + \frac{g^2}{(4\pi)^2}\left[\frac{5N_c + 2N_f(1-4\ln 2)}{3} + \frac{11-2N_f}{3}L_b\right]\right)(m_D^{LO})^2 - C_F N_f \frac{g^4}{(4\pi)^2}, \tag{5.1}$$

where L_b is the bosonic Matsubara sum. Moreover we use the NLO field renormalization factor Z_1,

$$Z_1 = 1 + \alpha_s\left[\frac{11N_c}{3}(L_b+1) - \frac{2N_f}{3}(L_f-1)\right], \tag{5.2}$$

with bosonic and fermionic Matsubara sums $L_b = 2\ln\left[\mu e^{\gamma_E}/(4\pi T)\right]$ and $L_f = 2\ln\left[\mu e^{\gamma_E}/(\pi T)\right]$. α_s, m_D and Z_1 explicitly depend on the renormalization scale μ. The NLO results for the subtracted free energies read

$$\begin{aligned} F_S^{\mathrm{sub,NLO}} = &-C_F\frac{\alpha_s(\mu)e^{-rm_D(\mu)}}{r}\Big(Z_1^2(\mu,T) \\ &+ \alpha_s(\mu)N_c rT\left[2 - \ln\left(2rm_D(\mu)\right) - \gamma_E + e^{+2rm_D(\mu)}E_1(2rm_D(\mu))\right]\Big), \end{aligned} \tag{5.3}$$

$$\begin{aligned} F_{Q\bar{Q}}^{\mathrm{sub,NLO}} = &\left\{\frac{\alpha_s(\mu)e^{-rm_D(\mu)}}{3rT}\right\}^2\Big(Z_1^2(\mu,T) + 2N_c\alpha_s(\mu)rT\left[\frac{3-\gamma_E}{2} + \frac{\ln[rm_D(\mu)]}{2} - \ln[2rm_D(\mu)]\right. \\ &\left. + \frac{\ln[2rm_D(\mu)]+\gamma_E}{rm_D(\mu)} - \frac{1}{2}g[2rm_D(\mu)] + \frac{1}{2}h[4rm_D(\mu)] - \frac{h[2rm_D(\mu)]}{rm_D(\mu)}\right]\Big), \end{aligned} \tag{5.4}$$

where the functions $g(y)$ and $h(y)$ are defined as

$$g(y) = \int_0^\infty dx\,\frac{e^{-xy}}{x+1}\ln\left[\frac{x+2}{x}\right], \qquad h(y) = e^y E_i(-y). \tag{5.5}$$

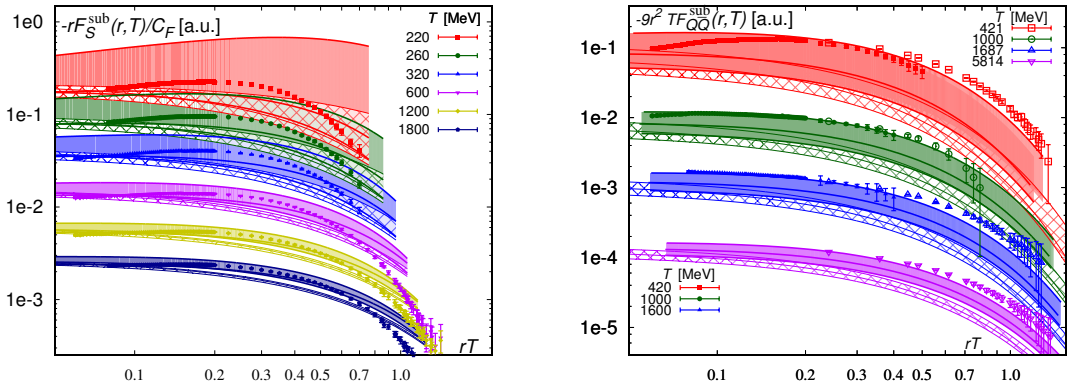

Figure 6: Subtracted free energies from lattice and EQCD. Hashed or solid bands represent the EQCD results at LO or NLO respectively for a variation of the cutoff scale as $\mu = \pi T$, $2\pi T$ and $4\pi T$. For $F_{Q\bar{Q}}$ we show continuum results as filled symbols and $N_\tau = 4$ results with $N_\sigma/N_\tau = 6$ as open symbols (right).

The second power of first term in Eq. (5.4) is due to the cancellation between color-singlet and color-adjoint contributions discussed already in Eq. (4.6).

We show continuum-extrapolated lattice results for the subtracted free energies together with the EQCD predictions at LO and NLO in Fig. 6. The lattice results are much better described by EQCD at NLO than at LO, indicating that the weak-coupling expansion is indeed on solid footing in the electric screening regime. For small ($rT \ll 0.2$) and large ($rT \gg 0.4$) separations the rT dependence of F_S is not consistent with EQCD. We understand the former as the vacuum-like regime, for which pNRQCD provides an appropriate description, cf. Sec. 4. We understand the latter as the regime of asymptotic screening. The corresponding asymptotic screening mass is considerable larger than the Debye mass of EQCD. At small rT we see a non-EQCD regime in $F_{Q\bar{Q}}$, too. The rT dependence in this regime, which rapidly becomes shorter with increasing temperature, is inconsistent with EQCD. From Sec. 4 we understand that the spectral gap is still large in this vacuum-like regime. With available lattice data we cannot resolve the onset of a regime of asymptotic screening in $F_{Q\bar{Q}}$.

6. Asymptotic screening regime

In the asymptotic regime screening is dominated by the magnetostatic scale g^2T. Whereas g^2T is formally smaller than the electrostatic Debye mass scale gT, it turns out to be more important numerically for any physically relevant values of the temperature and the gauge coupling. The magnetic mass $m_M \sim g^2T$ in turn leads to a breakdown of weak-coupling power counting in diagrammatic descriptions [9]. As a consequence, this regime is inherently non-perturbative.

Long range interactions contributing to the free energies are dominated by one-particle-exchange processes, thus giving rise to a Yukawa-type interaction $\sim \exp[-Mr]/r$ for a mode of mass M. In the case of C_P these OPE processes concur in some intermediate regime (between electrostatic and magnetostatic regimes) by two-particle-exchange processes $\sim \{\exp[-Mr]/r\}^2$.

For multiple reasons we cannot simply study asymptotic screening through a straightforward fit with Yukawa potential at large values of r. First we have to account for finite volume corrections

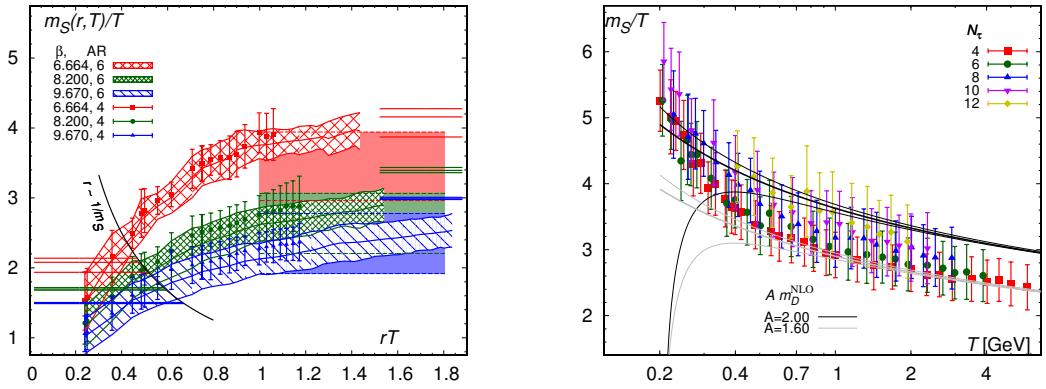

Figure 7: Asymptotic screening mass for F_S. We observe no statistically significant volume dependence of m_S/T, which is for $r \sim 1/m_s$ close to the NLO Debye mass m_D (horizontal lines from left). m_S/T stays somewhat below $2m_D/T$ (horizontal lines from right) in the accessible range for $N_\tau = 4$ (left). The corrected values of m_S/T are shown as solid bands in the left panel and as function of T in the right panel.

since cancellations in Eqs. (2.5) and (2.6) are exact only in infinite volume and may be limited by statistics. In fact we see a volume dependence by comparing screening functions $S_1 = -rF^{\text{sub}}$ with aspect ratios $N_\sigma/N_\tau = 6$ and $N_\sigma/N_\tau = 4$. Volume dependence is reduced for larger ensembles and we successfully model it as a constant offset that we subtract from correlators to bring results for different aspect ratios into numerical agreement. Second we cannot determine the asymptotic screening mass through a straightforward fit in the far asymptotic regime due to an exponential drop of the signal-to-noise ratio. Instead we have to start fitting at intermediate rT values for which the system is not necessarily beyond the electric screening regime. Hence, we fit F_S^{sub} and $F_{Q\bar{Q}}^{\text{sub}}$ as

$$F^{\text{sub}}(rT,T,a) = A\frac{e^{-MR}}{R} + C,\ R \equiv rT \tag{6.1}$$

and vary both small (R_{min}) and large (R_{max}) ends of the fit range to obtain a local definition of the screening mass $M = m/T$.

In the case of F_S the parameter $M(R_{\text{min}}, R_{\text{max}})$ is a monotonically rising function of R_{min} and R_{max} that becomes considerably flatter for $R_{\text{min}} \gg 0.7$. Since the dependence on R_{max} is rather mild we average for fixed R_{min} over all R_{max} that permit good fits for Eq. (6.1) and estimate a systematic uncertainty from the spread. Even for F_S^{sub} with $N_\sigma/N_\tau = 6$ we still observe a non-negligible increase even for the largest R_{min}, cf. left panel of Fig. 7. For $N_\sigma/N_\tau = 4$ we are not even able to obtain a stable screening mass for $R_{\text{min}} \gg 0.7$ in many cases. For $R_{\text{min}} \sim 1/m_D$ the screening mass is close to the NLO Debye mass, while for $rT \gg 1$ the screening mass remains below twice the NLO Debye mass. We estimate a temperature independent additive correction between the parameter M for $R_{\text{min}} = 0.5$ and for $R_{\text{min}} \gtrsim 1.0$ and take the corrected result as our estimate of the asymptotic screening mass. We plot this corrected value of the screening mass as function of the temperature in the right panel of Fig. 7. Although there is a trend to larger values of M towards the continuum limit, screening masses for all N_τ are numerically commensurable. The temperature dependence for $T > 400\,\text{MeV}$ and the N_f dependence are consistent with the NLO Debye mass.

In the case of $F_{Q\bar{Q}}$ the parameter $M(R_{\text{min}}, R_{\text{max}})$ exhibits no statistically significant dependence on either R_{min} and R_{max} beyond $R_{\text{min}} \gtrsim 0.5$. For $N_\tau = 4$ and $N_\sigma/N_\tau = 6$ we find a monotonic

T [MeV]	421	1687	5814
$m_{Q\bar{Q}}/T$	4.6(1)	4.2(3)	3.9(2)

Table 1: The screening mass of $F_{Q\bar{Q}}$ for $N_\tau = 4$ and $N_\sigma/N_\tau = 6$ for $R_{\min} = 0.5$.

decrease of $m_{Q\bar{Q}}/T$ with temperature, see Tab. 1.

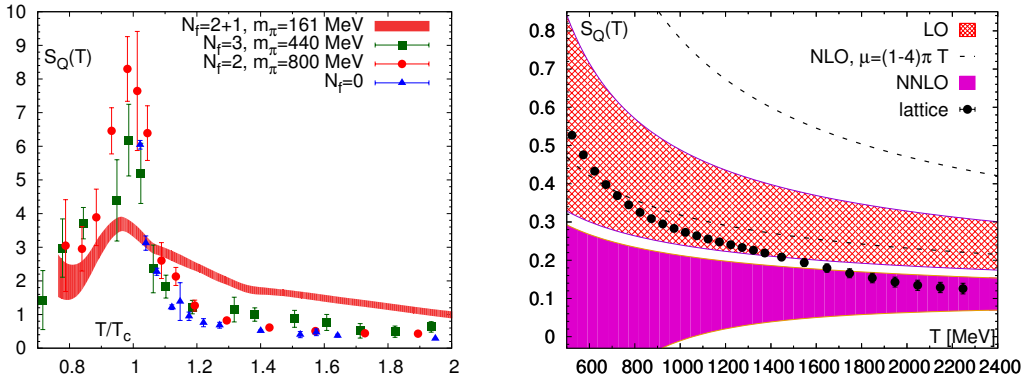

Figure 8: The entropy S_Q of a static quark is sensitive to the color screening and deconfinement.

Asymptotically separated quarks eventually decouple completely and any quark-antiquark free energy approaches $2F_Q$. We study this asymptotic regime in terms of the entropy of a static quark,

$$S_Q = -\frac{dF_Q}{dT}, \tag{6.2}$$

which is renormalization-scheme independent in the continuum limit. As the entropy is at leading order $S_Q^{\mathrm{LO}} = C_F \alpha_s(\mu) m_D^{\mathrm{LO}}(\mu)/(2T)$, it is a direct probe of the color screening properties of the thermal QCD medium. S_Q is peaked in the crossover region and the peak position $T_S(N_\tau)$ is numerically consistent with the peak position $T_\chi(N_\tau)$ of the chiral susceptibilities on the same set of ensembles. This suggests that the critical temperatures related to the phase transitions in the opposite corners of the Columbia plot are smoothly connected, since the entropy and chiral susceptibilities are primarily sensitive to different aspects of the crossover transition. For lower quark masses or larger N_f, the peak of S_Q is less pronounced, cf. the left panel of Fig. 8, suggesting that the peak may indeed be washed out completely for ensembles close to the chiral limit.

The Polyakov loop and the entropy have been calculated up to NNLO [16]. We have made an order-by-order comparison to lattice results with $N_\tau = 4$ [6], seeing remarkably poor convergence at NLO. This can be understood as a consequence of the dominance of the static Matsubara mode in S_Q. First indications of consistency between NNLO and lattice results for $N_\tau = 4$ were seen for $T \gtrsim 3\,\mathrm{GeV}$. With the new ensembles we extend the continuum limit to $T \gtrsim 2\,\mathrm{GeV}$ and find consistency with NNLO already for much lower temperatures, $T \gtrsim 1.7\,\mathrm{GeV}$ as shown in the right panel of Fig. 8.

7. Conclusions

We study color screening in the quark-gluon-plasma with lattice QCD and weak-coupling approaches. We extract the continuum limit of the Polyakov loop correlator and related quantities

in an unprecedented range up to $T \gtrsim 2\,\mathrm{GeV}$ and perform detailed comparisons to different effective field theory results at weak coupling. We successfully identify a vacuum-like regime, an electric screening regime and an asymptotic regime and establish a direct connection to the weak-coupling calculations and the realization of the assumed hierarchies of scales.

Acknowledgments

We acknowledge the support by the Bundesministerium für Bildung und Forschung (BMBF) under grant "Verbundprojekt 05P2015 - ALICE at High Rate (BMBF-FSP 202) GEM-TPC Upgrade and Field theory based investigations of ALICE physics" under grant No. 05P15WOCA1. The simulations have been carried out on the computing facilities of the Computational Center for Particle and Astrophysics (C2PAP) and Supermuc. The data analysis was performed using the R statistical package.

References

[1] A. Bazavov, PoS LATTICE **2014**, 392 (2015).

[2] P. Petreczky, J. Phys. G **39**, 093002 (2012) [arXiv:1203.5320 [hep-lat]].

[3] Preprint TUM-EFT 81/16: A. Bazavov, N. Brambilla, P. Petrèczky, A. Vairo, J. H. Weber, "Color screening in 2+1 Flavor QCD".

[4] A. Bazavov *et al.*, Phys. Rev. D **85**, 054503 (2012) [arXiv:1111.1710 [hep-lat]].

[5] A. Bazavov *et al.* [HotQCD Collaboration], Phys. Rev. D **90**, 094503 (2014) [arXiv:1407.6387 [hep-lat]].

[6] A. Bazavov, N. Brambilla, H.-T. Ding, P. Petreczky, H.-P. Schadler, A. Vairo and J. H. Weber, Phys. Rev. D **93**, no. 11, 114502 (2016) [arXiv:1603.06637 [hep-lat]].

[7] A. Bazavov, P. Petreczky and J. H. Weber, arXiv:1710.05024 [hep-lat].

[8] M. Berwein, N. Brambilla, P. Petreczky and A. Vairo, Phys. Rev. D **96**, no. 1, 014025 (2017) [arXiv:1704.07266 [hep-ph]].

[9] S. Nadkarni, Phys. Rev. D **33**, 3738 (1986).

[10] N. Brambilla, J. Ghiglieri, P. Petreczky and A. Vairo, Phys. Rev. D **82**, 074019 (2010) [arXiv:1007.5172 [hep-ph]].

[11] B. A. Kniehl, A. A. Penin, Y. Schroder, V. A. Smirnov and M. Steinhauser, Phys. Lett. B **607**, 96 (2005) [hep-ph/0412083].

[12] P. Petreczky and H.-P. Schadler, Phys. Rev. D **92**, no. 9, 094517 (2015) [arXiv:1509.07874 [hep-lat]].

[13] E. Braaten and A. Nieto, Phys. Rev. D **51**, 6990 (1995) [hep-ph/9501375].

[14] E. Braaten and A. Nieto, Phys. Rev. D **53**, 3421 (1996) [hep-ph/9510408].

[15] Y. Burnier, M. Laine and M. Vepsalainen, JHEP **1001**, 054 (2010) Erratum: [JHEP **1301**, 180 (2013)] [arXiv:0911.3480 [hep-ph]].

[16] M. Berwein, N. Brambilla, P. Petreczky and A. Vairo, Phys. Rev. D **93**, no. 3, 034010 (2016) [arXiv:1512.08443 [hep-ph]].